www.rericjournal.ait.ac.th

Study of Building Effects on Small HAWTs Performance in Building - Obstructed Wind Flow Area by using a CFD k-ε Turbulence Model Validated with Site Measurement

Krittapas Kongkapisuth*[1], Wirachi Roynarin*, and Decha Intholo*

Abstract – *The power performance of small wind turbines (SWTs) in a building-obstructed wind-flow area faces significant challenges such as highly turbulent wind flow, low wind speed, etc., that can affect the wind power utilization. Therefore, it is necessary to ascertain the power performance in such areas before installing SWTs by using processes that are simple, reliable, and economical to reduce the invested cost and time. Using computational fluid dynamics (CFD) techniques is one such process. In this study, three rotational 5-kW horizontal-axis wind turbines (HAWTs), WT1, WT2 and WT3 which are located in the Defense Energy Training Center (DETC) in Rayong Province, Thailand, are studied to explore the influence of the wind-flow on them. The objective of this study is to investigate the effectiveness of the HAWTs' power performance as the wind flows across the obstructive buildings in the DETC from two directions, namely the north-east (NE) and the south-west (SW), by using a CFD k-ε turbulence model and to validate the model with the data measured on the site with free spinning rotor condition as the wind flows from the SW. From the results of the CFD simulation, which were compared with the results from the WT0 (a wind turbine without obstruction, at an incoming wind speed of 4.5 m/s), it was found that as the wind flowed from the NE, the free spinning rotating of WT1–WT3 increased by 39.12%, 26.47%, and 28.53% respectively. As wind flowed from the SW, the free spinning rotating of WT1 and WT2 increased by 7.73%, and 5.68%, respectively, while, the free spinning rotating of WT3 decreased by 7.50%. Hence, when the wind flows from different directions, the free spinning rotating of the WT1–WT3 from the NE are higher than the wind flowed from the SW by 31.39%, 20.79%, and 36.03%, respectively. From the results of the site measurement as the wind flows from the SW, it is observed that at an incoming wind speed of 4.5 m/s, the free spinning rotating of WT1 > WT3 > WT2, while from the CFD analysis, the free spinning rotating of WT1 > WT2 > WT3. Consequently, this study investigated that the wind flow in such area causes both increased and decreased power performance of the SWTs.*

Keywords – computational fluid dynamics (CFD), building-obstructed wind flow, small horizontal axis wind turbines (small HAWTs), k-ε turbulence model.

1. INTRODUCTION

Renewable energy resources, such as solar, wind, hydro, tides, waves, geothermal, and biomass, are replenished by nature. Generally, these alternative energy sources can provide electrical, thermal, fuel, and off-grid energy. According to the REN21's (the Renewable Energy Policy Network for the 21st Century) 2016 report, renewable energy utilisation accounts for about 8.9% of the world's energy needs, and 2.2% of this renewable energy supply is used for electricity production and is generated from wind, solar, geothermal, and biomass sources [1]. Currently, the world's energy consumption is continuously increasing and renewable energy has the potential to supply an abundant amount of clean energy, if the resources are harnessed efficiently [2].

1.1 Wind Energy

Wind energy has been identified as a reliable source of renewable energy. A wind turbine (WT) is a device that converts the wind's kinetic energy into electrical power. Wind turbines are usually installed based on an accurate or approximate study of wind resources; however, the design is constrained by socio-economic and environmental concerns. Most suitable sites for the wind turbines are the windy areas far from the obstacles to the wind flow. Small horizontal-axis wind turbines (HAWTs) can be used to fulfill the energy needs of urban societies. Their production can also be harnessed to support the on-grid and off-grid applications [3]-[6].

The turbulent flow, which involves chaotic changes in pressure and flow velocity, is a common phenomenon in wind energy and is often characterized by unsteady wind turbine performance [7]. Turbulent flow consists of the irregular swirls of fluctuations that occur in three dimensions: along-flow (steam-wise), across flow (cross-stream), and vertical. Turbulence is caused not only by obstacles but also by the topography of the landscape. Therefore, it is necessary to investigate the effects of the turbulence intensity and vortices on the wind turbines for improved power performance of any intended installation [8]. One challenge for small wind turbines in such areas is the low energy yield resulting from a low mean wind speed because of the eddies and the swirls. Turbulence also hinders the performance of wind turbine performance because the wind profiles in such areas are different from the open areas [9],[10]. Examples of turbulent and laminar flow are shown in Figure 1. The wind speed distribution depends on the type of air flow in the atmospheric boundary layer and varies as a function of the altitude and the site topography.

*Engineering Faculty, Rajamangala University of Technology Thanyaburi, Phathumthani, Thailand 12110.

[1]Corresponding author;
Tel: + 66095 820 7960.
E-mail: krittapas_k@mail.rmutt.ac.th.

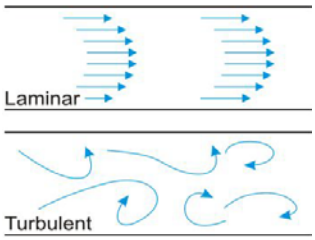

Fig. 1.Turbulent and laminar flow [10].

Figure 2 shows the wind flow being deflected from its path upon encountering an obstacle. The wind flows around the obstacle, accelerating as it passes around the sides and over the top, and creates a slower and more turbulent wind area that continues for a distance behind the obstacle [11].

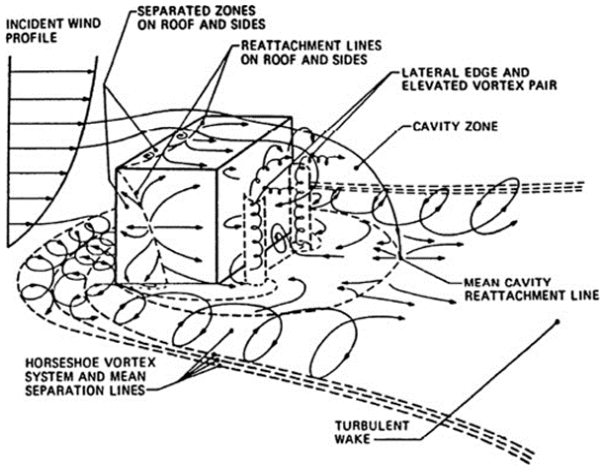

Fig. 2. Waked flow across of obstacle [11].

Wind turbines are designed to perform very efficiently; however, building-obstructed airflow can cause wind flow impedances, leading to inefficiency and irregularity. The behavior of a WT in the field is affected by the wind speed and the wind flow direction. With each change of the direction and the speed, the turbine will try to adapt to the new conditions; however, this transition usually reduces the energy production. In other words, the reasons behind the limited installation of small wind turbines in building-obstructed wind-flow areas are the low mean wind speeds and the high level of turbulence encountered in those scenarios [12]. Therefore, before installing wind turbines in such areas, a proper analysis and performance prediction is necessary. This can be estimated using computational fluid dynamics techniques that are simple, accurate and cost and time effective [13].

Many researchers have investigated the effects of the turbulence force on the wind turbine, such as the high turbulence intensity of the wind and increased fatigue and reduced lives of the wind turbines. The impact of the atmospheric and wake turbulence on wind turbine fatigue loading was investigated[14] using large eddy simulations of the atmospheric boundary layers [15] confirmed that harsh climatic conditions and complex terrain could affect both the energy output and the steady and fatigue loading on wind turbines.

High ambient turbulence intensities, defined along the direction of the mean wind speed, can have a detrimental effect on the aerodynamic performance of the blades mostly due to the stalled conditions that can lead to a ‘‘branching’’ of the power curve,[16]. At high transversal turbulence intensities, the horizontal plane is at a perpendicular direction to the longitudinal turbulence intensity; hence, the turbine cannot align along the gusting wind [17]. All these factors, which influence the power output of small sized wind turbines, can be mitigated with technical improvements of the control system to obtain a faster response to the high wind speed variability. However, these effects are not considered in the standards for wind turbine power curve testing [18], thus limiting the applicability of the standard power curves for realistic resource assessment. Recently, a new approach has been suggested, allowing the normalisation of the wind turbine curve data to the turbulence intensity at the site, by comparing the measured and the corrected power curves of the turbines.

1.2 Turbine Performance

The expected turbine performance is demonstrated by the manufacturer’s power curve. The manufacturer’s power curve is typically derived from the test data in ideal wind conditions. The data from non-ideal wind conditions are filtered out of the analysis, so that results demonstrate the turbine’s performance when subjected to un-waked horizontal non-turbulent flow at sea-level air density.

Although some installation site parameters may be close to the ideal conditions, others, particularly those in the urban environments, will exhibit less ideal conditions. This is proved by the lower power production at these locations, indicated by a drop in the manufacturer’s power curve. A comparison between the measured power curves and the application of the procedure by Figure 3 [19] presents an example of the power curve and demonstrates energy production. Therefore, the expected energy production at turbine locations requires adjustment to reflect the performance dependence on real conditions experienced at the site. The small sized wind turbines are expected to have a faster response to changes in the wind compared to the large sized ones [20].

The performance variables are the turbine power P and overall turbine system efficiency η. These two variables can be combined with two unknowns to describe a general turbine system as follows:

$$P = \eta T \omega \quad (1)$$

where T and ω are the torque and angular velocity of the wind turbine rotor.

Figure 3 shows the nominal power curve provided by the manufacturer (represented by the dashed lines) and the measured power curves in the site (represented by the solid lines), while the blue symbols are scattered, as expected, around the measured power curves.

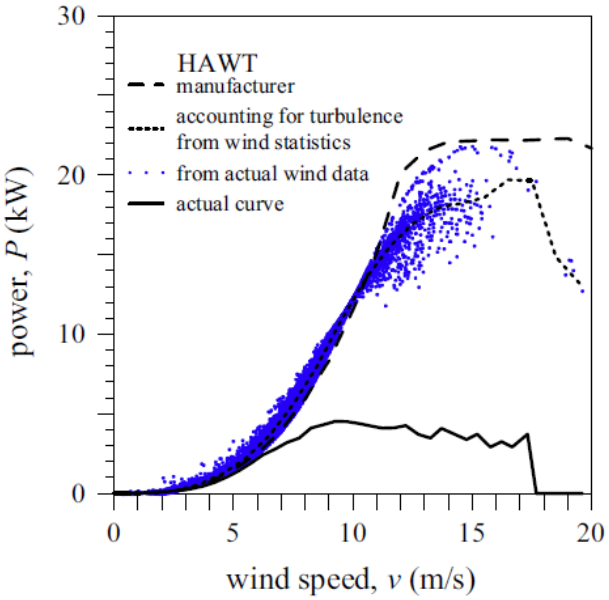

Fig. 3. Power curve of HATW between manufacturer and site installation[19].

1.3 Turbulence

For a steady turbulent shear flow, the mean velocity profile in a small region near the surface is described by a relationship called the Wall law:

$$\frac{u_t}{u^*} = \frac{1}{2} ln\left(\frac{z}{z_0}\right) + B \qquad (2)$$

where u^* is the friction velocity and B is an empirical constant related to the thickness of the viscous sublayer (B = 5.2 in a boundary layer over a smooth flat plane, for rough walls, smaller values of B are obtained) [21]. The constant z_0 is called the roughness and is the frontier between the logarithmic zone and the inner $k-\varepsilon$ zone. When the wind speed changes direction with increasing height above the ground, it is called the shear gradient. The wind-shear formula is shown below:

$$U = U_{ref}\left(\frac{h}{h_{ref}}\right)^{\alpha} \qquad (3)$$

where U and U_{ref} represent the wind speed at heights h and h_{ref}, respectively and; h and h_{ref}, in turn, represent the height of the interest and the reference height, respectively. Finally, α represents the site/condition-specific shear exponent.

1.4 Simulation Method

Computational fluid dynamics (CFD) methods are constantly being developed to improve the computational resource capability. CFD has reached a stage where the analysis of complex phenomena such as multiphase, free surface, and highly turbulent flows is possible for a large number of design variations in a reasonable timescale [22]. Recent developments of the CFD codes have shown that the simulation of this nature is in good agreement with experimental data [23], thereby proving that the numerical results are reliable. This paper presents the results of the CFD simulation of rotation on free spinning condition of three 5-kW HAWTs in a building-obstructed wind-flow area at the DETC. The results of the CFD simulation are compared with the measured data of the rotor rotating, free spin, of the turbines. In the CFD conditions, CFD k-ε turbulence model is used for simulating the performance effect of three 5-kW HAWTs with the hub height of 18 m and the blade diameter of 6.4 m that be installed among the four main concrete buildings at the heights of 9.25 m, 13.30 m and 15.0 m respectively, as the wind flows across the buildings obstruction from two directions (the North-East (NE) and the South-West (SW)). It is noted that these wind flow directions are common in Thailand.

This paper presents the results of the *free spinning rotating* effect of three 5-kW HAWTs located in the DETC in a building-obstructed wind-flow area in Rayong province, Thailand, using the CFD k-ε turbulence model validated with site measurement base on measured data.

2. COMPUTATIONAL FLUID DYNAMICS

Computational fluid dynamics (CFD) is a fluid mechanics simulation for solving and analysing fluid flows. It can be applied to predict wind-turbine performance accurately at minimum or optimum cost and time scale. The CFD results can be compared with the experimental results. In the computational modelling of turbulent flows, an appropriate model that complies with the obstruction type can predict the fluid velocity and other relevant issues for engineering designs involving fluid flows [24].

A CFD turbulence model has the procedure to close the system of mean flow equations. It is not necessary for engineers to resolve the details of the turbulent fluctuations. They only need to know how the turbulence affects the mean flow. Useful turbulence models must have wide applicability and must be accurate, simple and economical to run. Most classical models are based on the Reynolds-averaged Navier–Stokes (RANS) equations (time averaged), for example, zero equation models, mixing length models, one-equation models, two-equation models, k-ε style models

(standard, re-normalisation group (RNG), realizable), k-ω models, etc. [25].

The Reynolds-averaged approach is based on decomposing the velocity as

$$u_j = \overline{u_j} + \acute{u_j} \tag{4}$$

where $\overline{u_j}$ is the average velocity vector and $\acute{u_j}$ is the velocity vector fluctuation. The $k-\varepsilon$ model has been found to provide a more effective response to the energy production rate than the standard $k-\varepsilon$ turbulence model. The $k-\varepsilon$ model equations can be written as follows:

$$\rho(\overline{U}.\nabla)K = \nabla\left[\left(\mu + \frac{\mu_t}{\sigma_k}\right)\nabla K\right] + P_k - \rho\varepsilon \tag{5}$$

$$\rho(\overline{U}.\nabla)\varepsilon = \nabla\left[\left(\mu + \frac{\mu_t}{\sigma_\varepsilon}\right)\nabla\varepsilon\right] + C_{\varepsilon 1}\frac{\varepsilon}{K}P_k - C_{\varepsilon 1}\rho\frac{\varepsilon^2}{K} \tag{6}$$

$$\mu_t = \rho C_\mu \frac{K^2}{\varepsilon} \tag{7}$$

$$P_k = \mu_t[\nabla\overline{U} + (\nabla\overline{U})^t]\nabla\overline{U} \tag{8}$$

The standard model constants, which are applicable to the flows with high Reynolds numbers, are provided in Table 1. The CFD k-ε turbulence model is selected to validate the performance prediction of the turbine as the characteristics of the CFD k-ε turbulence model are most appropriate for the given conditions of the study:

- The CFD $k-\varepsilon$ turbulence model is the most widely used model and has been validated for the applications ranging from the industrial to the environmental flows.
- The model is useful for the free-shear layer flows with relatively small pressure gradients in the confined flows where the Reynolds shear stresses are important.
- The model can be stated as the simplest model for which only initial and/or boundary conditions need to be supplied.
- Two equations and the Von–Karman Constant (k) together with the eddy-viscosity stress-strain relationship constitute the k-ε model, where ε is the dissipation rate of k. Many attempts have been made to develop the two-equation models to improve the $k-\varepsilon$ model.

Table 1. Values of the $k-\varepsilon$ model constants.

C_μ	$C_{\varepsilon 1}$	$C_{\varepsilon 2}$	σ_k	σ_ε
0.09	1.44	1.92	1	1.3

However, CFD simulations are sensitive to a large number of computational parameters that must be set by the user. Hence, before doing any wind-study project, the computational results should be compared with the measured data for different discretization schemes. Additionally, each scheme must be tested against the multiple turbulence models with respect to the grid-dependency tests.

2.1 Governing Equations

The governing equations are based on three fundamental conservation principles: the continuity equation (or the conservation of mass), the momentum equation obtained by applying the Newton's law of motion to a fluid element, and the energy equation (conservation of energy) based on the first law of thermodynamics. The governing equations, including the Navier–Stokes equation, developed by M. Navier and G. Stokes in the first half of the 19th century, are presented in their most general forms below:

- Continuityequation

$$\frac{\partial\rho}{\partial t} + \nabla\cdot(\rho\vec{u}) = 0 \tag{9}$$

- Momentum equation

$$\Sigma F = ma \tag{10}$$

- Expressed as the Navier-Stokes equation:

$$\frac{\partial}{\partial t}(\rho\vec{u}) + \rho(\vec{u}\cdot\nabla\vec{u}) = -\nabla p + \nabla\cdot\tau + S_m \tag{11}$$

where the stress tensor τ is related to the strain rate by:

$$\tau = \mu\left(\nabla\vec{u} + (\nabla\vec{u})^T - \frac{2}{3}\delta\nabla\vec{u}\right) \tag{12}$$

- Energy equation

$$\frac{\partial}{\partial t}(\rho h_t) - \frac{\partial\rho}{\partial t} + \nabla\cdot(\rho\vec{u}h_t) = \nabla\cdot(\vec{u}\cdot\tau) + \vec{u}\cdot S_m + S_e \tag{13}$$

where the total enthalpy h_t is related to the static enthalpy h_s by

$$h_t = h_s + \frac{1}{2}\vec{u} \tag{14}$$

There are no analytical models for governing equations of the complex-flow geometries and the discretisation of the numerical series expansions. Partial differentials are carried out to approximate the solutions. This numerical technique is the underlying principle of the CFD. Assumptions are usually allowed to simplify the equations. Removing some parameters in some cases can help solve the entire equation. The fluid flow is assumed to be steady, isothermal and incompressible.

The CFD program used to simulate a finite-volume method was also used for the spatial discretisation of the governing equations. The numerical method should be validated. This study will compare it to the experimental method and the flow feature in a small wind turbine will be investigated.

2.2 Venturi Effect

The Venturi effect is named after Giovanni Battista Venturi (1746–1822), an Italian physicist. The Venturi effect is the reduction in the fluid pressure that happens when a fluid flows through a constricted section. Analysis shows that in a situation with constant

mechanical energy, the velocity of a fluid passing through a constricted area will increase and its static pressure will decrease. This phenomenon utilises the continuity equation and the principle of conservation of mechanical energy and can be observed in both nature and industry. The Venturi effect increases the speed of a fluid when it funnels through small openings. The severity of the Venturi effect is a function of the width, length, height and size of the openings in the canyon. The Venturi effect is seen when winds accelerate while funneling through small openings. Both of these effects are explained by the Bernoulli's principle.

2.3 Building Features Effects

Building obstructed-wind flow inevitably causes irregular power performance of a wind turbine [26]. Normally, it causes small wind turbines harness little power from the wind resources because the building's obstruction environment usually has great turbulence and low velocity of wind flow. However, some features of the building environment can concentrate the wind flow; building edges, passage under the elevated structure or between the two buildings, etc. can enhance wind power utilization by increasing the wind power density.

The geometric features of the building structures and their layouts have major effect on the wind speed, direction, and frequency. Buildings can exert major frictional drag on the wind speed, which in turn creates turbulence and gives about abrupt changes in both direction and speed of the wind. The geometric features can slow the wind speed, but they can also channel the wind flow into building canyons beneath them that lead to an increase in the wind speed between the buildings (this effect is known as the Venturi effect) and can increase the frequency of the turbulent winds. In most case, buildings are narrowly spaced causing the wind flow between them to be interfered and leading to the increase in the wind speed.

2.3.1 Remark

In the CFD turbulence-model simulation, three rotational 5-kW HAWTs, with 18-m hub heights and 6.4-m blade diameters, are installed among four large concrete buildings with heights 9.25, 9.25, 13.30, and 15.0 m, with an incoming wind speed of 4.5 m/s.

3. MATERIALS AND METHODS

3.1 CFD Simulation Technique

This paper only focuses on the free spin rotation of the turbine rotor in both conditions, the CFD method and the experimental method, that affect three 5-kW HAWTs power performance from the wind flow. As the power performance of the wind turbines depends on the torque and angular velocity as described in equation 1. Hence, when the rotor turbine rotates, the voltage of the PMG generator will be generated and the voltage varies according to the rotational speed of the rotor; thus, high speed means high power.

3.2 Model Description

The site of study, the Defense Energy Training Center (DETC) in Rayong Province, Thailand, is considered as a building-obstructed wind-flow area. In this case, three 5-kW HAWTs, THUNYA-5 kW HAWTs (named WT1, WT2, and WT3), with the four main buildings are shown in Figure 4. The site position is latitude 12 degrees 40 minutes north, longitude 101 degrees 2 minutes east, and the height is 3 m above the sea level. The wind blows throughout the year, including the south-west monsoon season from May to October, and the north-east monsoon season from November to January. The statistical wind-speed data, collected over the past 30 years (between 1968 and 1997) in Rayong Province by the Data-Processing Division of the Department of Meteorology, shows that the average wind speed is between 2.6 and 7.7 m/s. The highest wind speed occurs between June and August. Table 2 describe the model, sizing and alignments of the buildings and wind turbines in the DETC, while Figure 5 shows the picture of the three wind-turbines (WT1, WT2, and WT3) along with the four main buildings A, B, C, and D in the DETC.

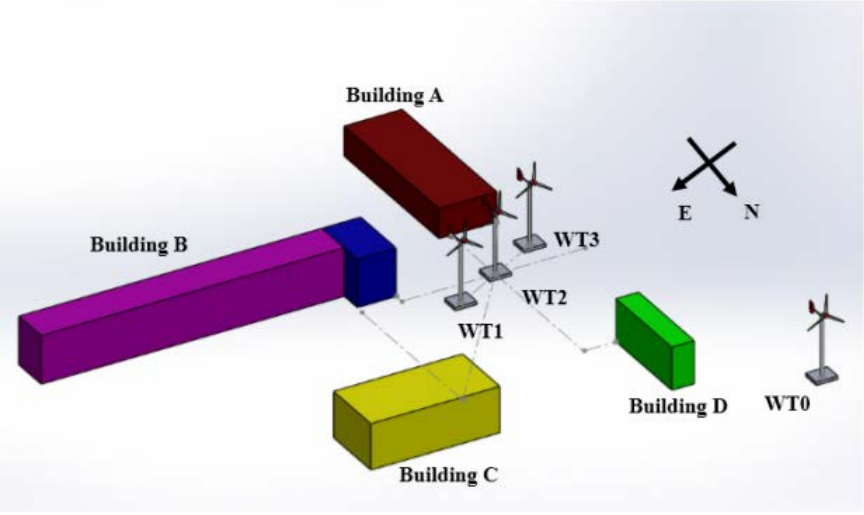

Fig. 4. Building model of the Defense Energy Training Center (DETC).

Fig. 5. Three 5-kW HAWTs in DETC.

Table 2. Sizing and alignment of the buildings and the wind turbines in DTEC.

Building	H (m)	W (m)	L (m)	Distance from WT1(m)	Distance from WT2(m)	Distance from WT3 (m)
A	9.25	18	51	35	24	20
B	15	12	113	25	30	45
C	9.25	18	51	60	70	87.5
D	13.30	7	30	47.5	50	55

Remarks: The wind turbines are 18 m apart. A three-dimensional model of the buildings and wind-resource data was used as input to the CFD model and completed using the CFDesign commercial program. Energy production data was obtained for the turbines and was compared to the results from the CFD power analysis, as well as the theoretical energy production. In this study, WT1, WT2, and WT3 represent the case-study 5-kW HAWTs, whose performance prediction is validated as the wind flows across the obstructing buildings, using the CFD k-ε turbulence model with the CFDesign V.7 software. The results of this study are expected to show the effectiveness (%) of the wind turbines' free spinning rotating compared to the power performance of WT0, a 5-kW HAWT arbitrarily located in a site without obstructing buildings, after an incoming wind flows at 4.5 m/s through the buildings.

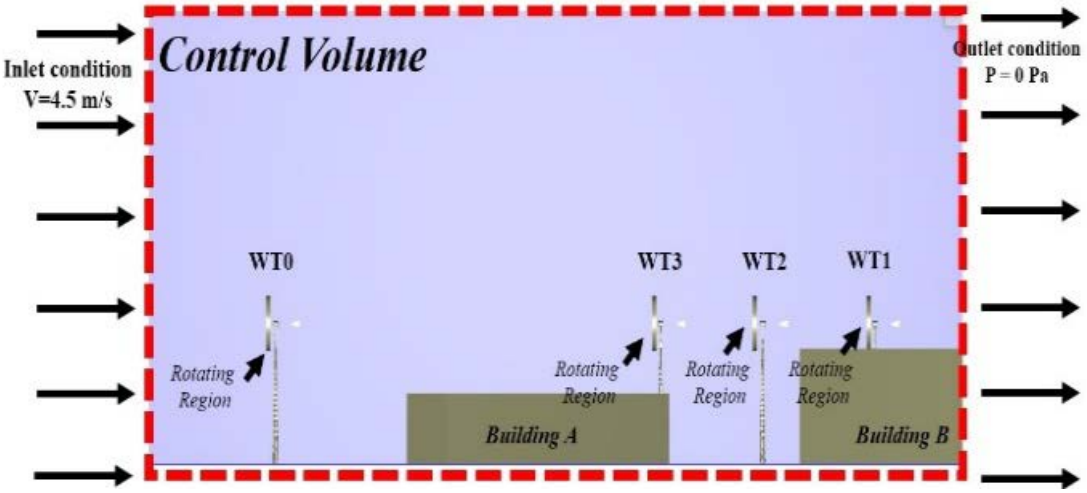

Fig. 6. CFD boundary conditions as the wind flows from the SW.

3.3 CFD Boundary Conditions

When solving the CFD problems, the Navier–Stokes equation, continuity equations, appropriate initial conditions and boundary conditions must be applied. Figure 6 shows the CFD boundary conditions of the 3D model applied as the control volume and using inlet k *and* ε turbulence for simulation of the wind flow from the SW directions. The model includes two main conditions: first, the buildings and the ground are fixed; second, the wind-turbine blades and the air are moving.

The fixed condition means the object or material in the 3D model cannot move when forces act on it (which include the building, ground, nacelle, wind turbine tower and wind turbine tailing), while the moving condition means that the object or material in the 3D model can move when forces act (which include the wind turbine blade, air and rotating region).

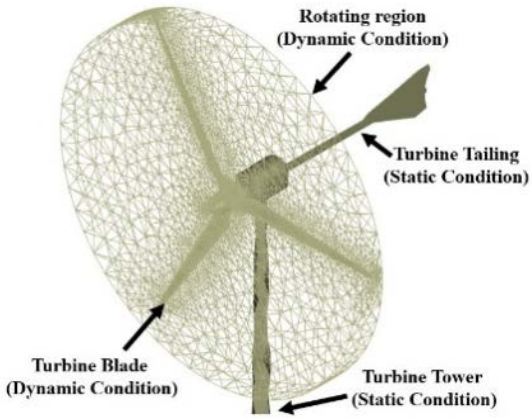

Fig. 7. Rotating region of the CFD boundary conditions.

Table 3. CFD model parameters.

Parameter name	Unit	Parameter Value
Inlet velocity	m/s	4.5
Inlet Total Temperature	K	320
Angular Velocity	Rad/s	Free spin
Working fluid		Ideal Air
Fluid Density	kg/m3	1.225
Turbulence Model		k-ε
Outlet	Pa	0

The rotating regions, which form a part of the motion module, allow for the analysis of rotating machinery. The rotating region is an envelope that surrounds a spinning device. Throughout the analysis, the rotating region rotates about its centerline and any solid within the region will rotate as well. The inlet condition of 4.5 m/s wind velocity is selected and the outlet condition is selected as 0 Pa of the wind gage pressure

Figure 7 describes the rotating region of the CFD boundary conditions, which include the moving/dynamic condition and fixed/static condition. The moving conditions include the rotating region and turbine blade, as both parts can move when the force of the wind velocity act on them. On the other hand, the fixed condition includes the turbine tailing and turbine tower as both parts cannot move when the force of wind act on them.

This model produces a steady-state solution accounting for some of the interaction between the two frames. The quasi-steady approximation decreases when the passing flow speed is large, relative to the turbine speed at the interface. The boundary conditions and control volume parameters are shown in Table 3.

Table 3 also shows the model parameters applied in the CFD control-volume model, with the inlet side selected by the wind velocity and the outlet side selected by the pressure. Ideal air was used as the working fluid and the k-ε turbulence model was applied for simulation.

CFD modelling was conducted to assess the wind flows and estimate the energy-output system, accounting for the specific geometries of the obstacle flows. The site geometry was modelled using computer-aided design (CAD). The wind conditions were expressed on the geometry model to estimate the flow conditions resulting from the interaction between the wind flow, building structures, ground roughness and wind turbines. A detailed explanation is presented below.

3.4 Model Description of Mesh Refinement Study

CFD uses an Eulerian fluid flow field specification. The domain is discretised using cell-vertex numerics (finite volume elements). These may be unstructured tetrahedral elements, which are used to capture the complex geometry of the rotating domains and to allow automatic meshing for any future geometry modifications. The CFD mesh-adaptation system was used to refine the mesh in specified high-volume velocity gradients for investigation. Three mesh-adaptation steps were undertaken for each model, called “coarse mesh’, ‘medium mesh’, and ‘fine mesh’.

Figure 8 shows the grid dependency of the 3D model at 4.5 m/s of wind velocity inlet condition. When the model is constructed with 0.25 million (coarse mesh) grid elements, the turbine has the rotation of 140 rpm, while the construction with 0.7 million grid elements (medium mesh) increases the rotation of the turbine to 168 rpm, but the curve in this period does not show convergence because the slope of curve is high. The curve shows convergence at the grid number of about 3.5 million elements (fine mesh) and the grid convergence at 4.5 m/s of the wind velocity inlet condition is shown in Table 4.

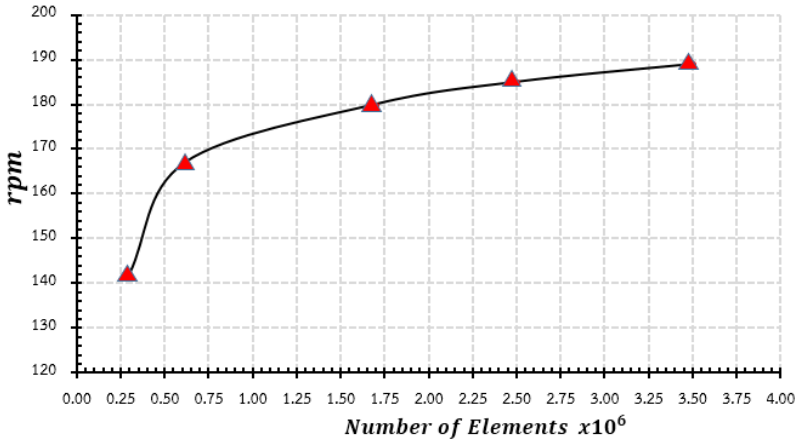

Fig. 8. Grid dependency of the 3D model at 4.5 m/s of wind velocity inlet condition.

Table 4. Grid convergence at 4.5 m/s wind velocity inlet condition.

Grid number × 10^6	Blade velocity (rpm)
0.25	141
0.50	162
0.75	170
1.00	172
1.50	178
2.50	185
3.50	189

Figure 9 shows the CFD tetrahedron meshing of the wind turbine blade. The CFD model generated 0.9 million elements for the wind turbine blade. Figure 9(a), 9(b) and 9(c) shows coarse mesh, medium mesh and fine mesh of the wind turbine blade, respectively.

(a) Coarse mesh (b) Medium mesh

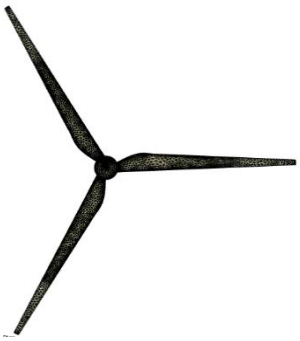

(c) Fine mesh

Fig. 9. Mesh of wind turbine blade in CFD.

Figure 10 shows the CFD tetrahedron mesh model of the buildings in the DETC. The CFD model generated 1.0 million elements for the buildings, 0.9 million elements for the wind turbine blade, 0.6 million elements for rotating region, 0.5 million elements for the air and 0.5 million elements for the ground.

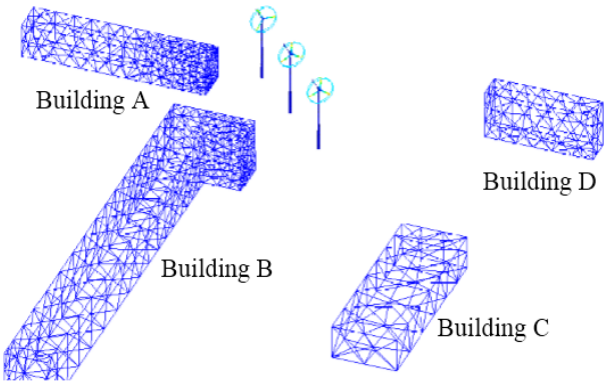

Fig. 10. Meshing of DETC buildings model.

3.5 Wind Turbine Specifications

Table 5 shows the technical data of a THUNYA-5kW HAWT, which is installed within the DETC area. The wind turbine is shown in Figure 11. The power curve of the wind turbine is shown in Figure 12, which describes the cut- in wind speed of the turbine at 2.5 m/s, the rated wind speed at 9.5 m/s. and the average wind speed at 4.5 m/s, the same the average wind speed in Thailand. In addition, Figure 13 shows the grid-connected inverter of the turbines in the electrical control room of the DETC.

Table 5. Technical data sheets of THUNYA-5K.

Main data	
Hub height	18 m
Rotor diameter	6.5 m
Rated power	5 kW @9.5m/s
Cut-in	2.5 m/s
Rotor speed	200 rpm
Generator Speed	200 rpm
Grid Connected	220 Volt 50 Hz
Rotor speed control	Fixed pitch
Yaw mechanism	Active (Azimuth angle)
Breaking system	Auto Furling

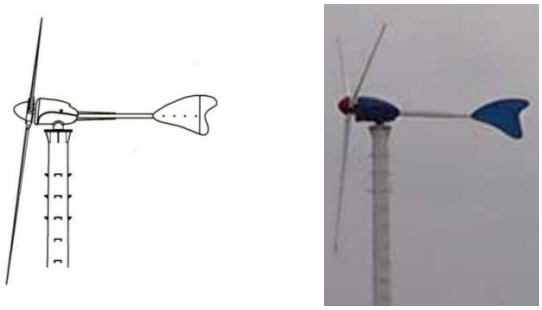

Fig. 11. THUNYA-5kW HAWTin DETC.

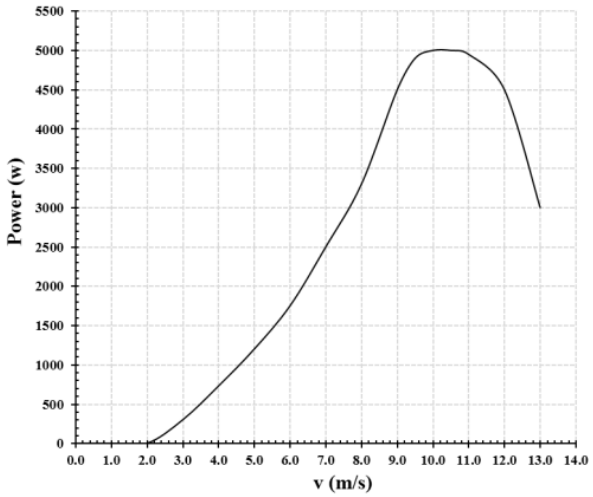

Fig. 12. Power curve of THUNYA-5kW HAWT.

Fig. 13. Grid-connected inverters of THUNYA-5kW HAWTs in electrical control room of DETC.

4. RESULTS AND DISCUSSION

4.1 CFD Simulation Results of Flow Modeling

Figures 14(a1)–(d2) show the wind-velocity profiles of the CFD results from two directions, the NE and the SW, at different heights, 9.25, 13.30, 15.0, and 18.0 m, of the cutting plane from the ground. The points of the cutting plane, representing the locations on the buildings' roofs, were determined by the inflow of the wind velocity, the turbulence intensity and the recirculation zones. The wind-velocity profile is indicated as follows: At the higher points of the cutting plane, there is more wind velocity and the wind flow from the NE is likely to introduce a Venturi effect near the buildings B-C and the buildings C-D, whereas the wind flow from the SW predominantly brings about a Venturi effect only from the buildings A-B and the buildings A-D. Moreover, at an 18.0 m wind-turbine hub-height, steep wind-shear gradients are obtained because of the building influences, causing an increased wind speed to the turbines.

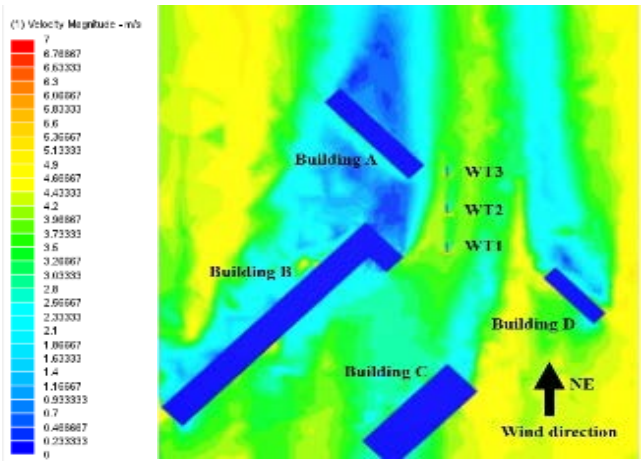

(a1) Height 9.25m, wind flow from NE

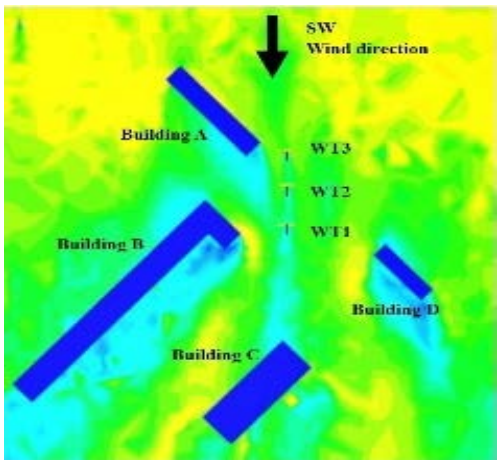

(a2) Height 9.25m, wind flow from SW

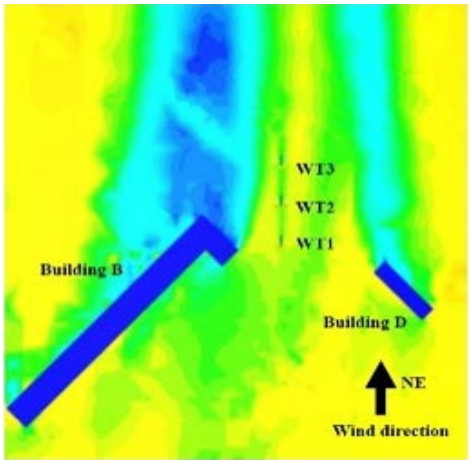

(b1) Height 13.30m, wind flow from NE

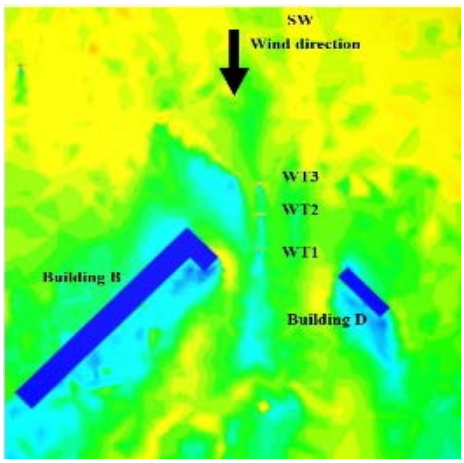

(b2) Height 13.30m, wind flow from SW

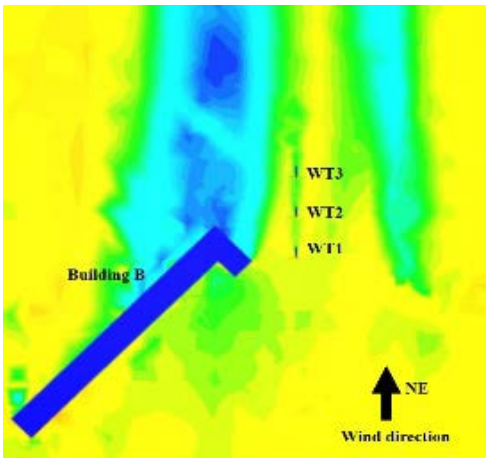

(c1) Height 15.0m, wind flow from NE

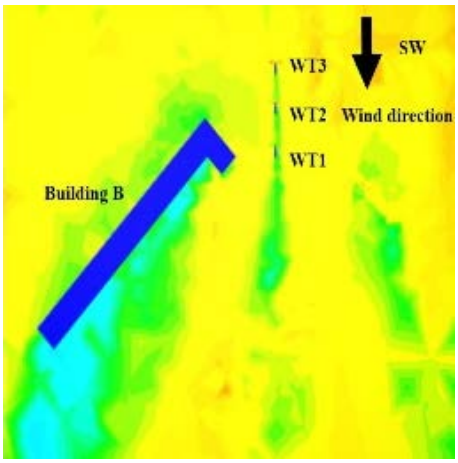

(c2) Height 15.0m, wind flow from SW

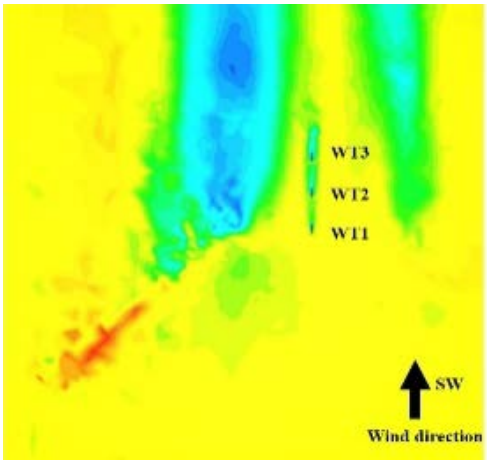

(d1) Height 18.0 m, wind flow from NE

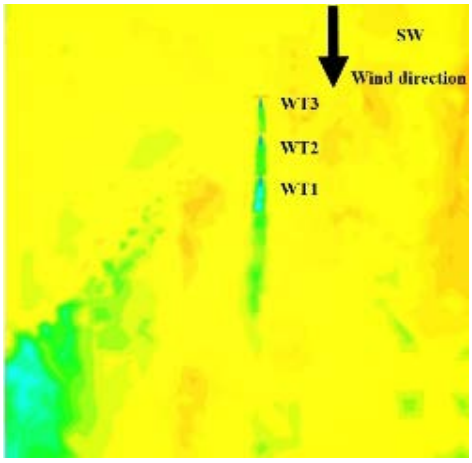

(d2) Height 18.0 m, wind flow from SW

Fig. 14. Wind velocity from two directions, the NE and the SW, at different heights from the ground (a) 9.25 m, (b) 13.30 m, (c) 15.0 m and (d) 18.0 m.

Figures 15(a) and (b) show that the DETC area has more open terrain from the SW; however, the wind-velocity contour from the NE across the buildings C and D to WT1-WT2-WT3 indicates that it is higher than the wind-velocity contour from the SW across the building A to WT3- building B- WT2-WT1 and across the C.

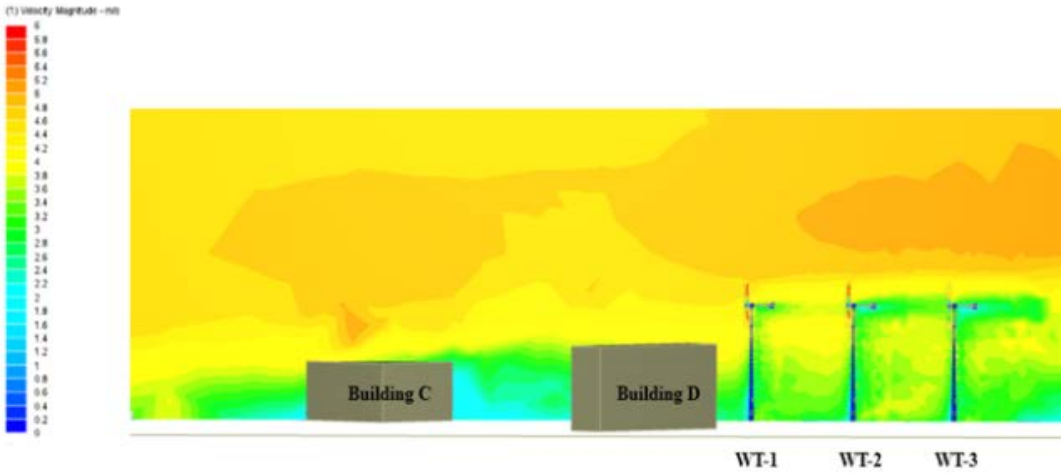

(a) Wind-velocity contour of wind flow from the NE

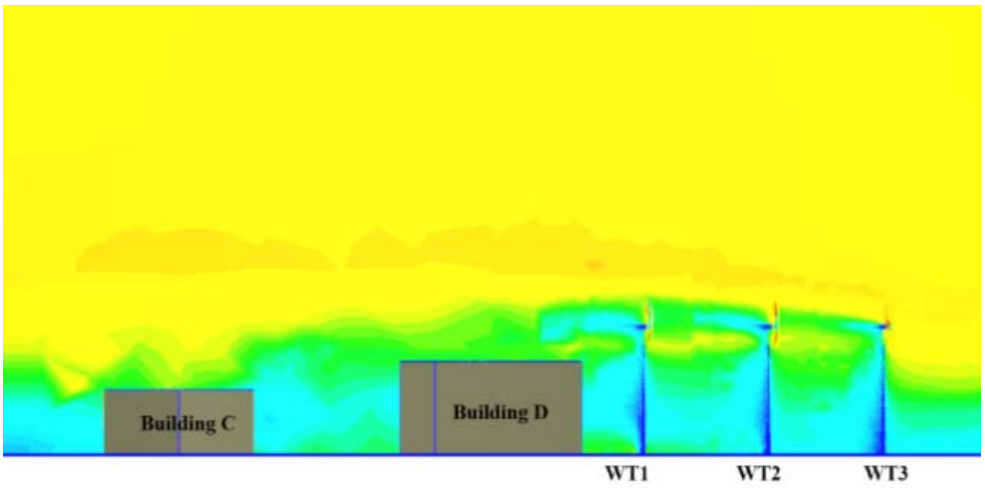

(b) Wind-velocity contour of wind flow from the SW

Fig. 15. Wind-velocity contour (a) from the NE; (b) from the SW.

Figure 16 shows the example of wind-velocity profile of air accelerating over the building C as the example at the height of 9.25 m. As the wind flow from the NE indicates, the roughness effect of the wind generates ground friction. The local wind-shear gradients can be generated above a roof surface as the wind flow passes over the building, leaving a low wind-speed region immediately above the roof and then transitioning steeply to a higher wind-speed zone. Therefore, steep wind-shear gradient are obtained because of the building influences, causing an increased wind speed to the turbine.

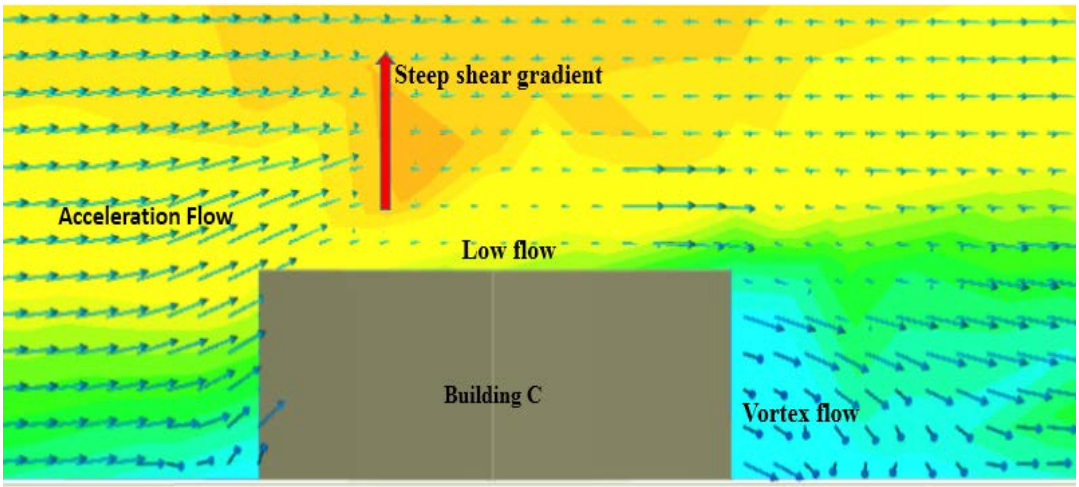

Fig. 16. Air accelerating over the building and creating a steep shear gradient.

Figures 17(a1)–(d) show the vortex-flow vectors at the wind turbines (WT1,WT2,WT3, and WT0) from the NE and the SW. The vortex is generated beside the WT1–WT3 because they are installed behind the buildings and the front turbines. When the air flows across the building, a vector direction of wind be changed that can be generated vortex beside WT1–WT3. The vortex flow is seen in the WT1–WT3, but no vortex flow is seen in the WT0, since it is an arbitrary installation in an unobstructed area.

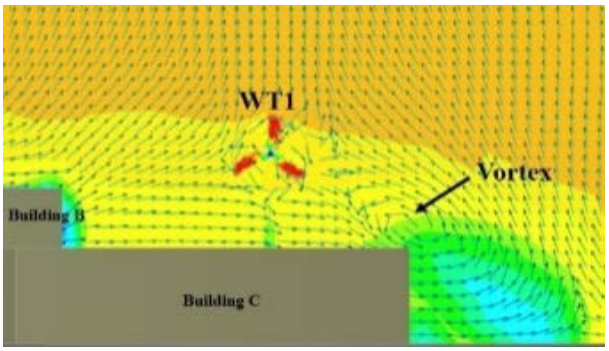

(a1) Vortex flow at WT1 as wind flows from NE

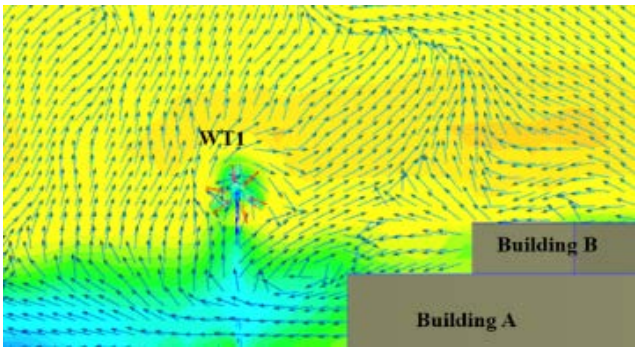

(a2) Vortex flow at WT1 as wind flows from SW

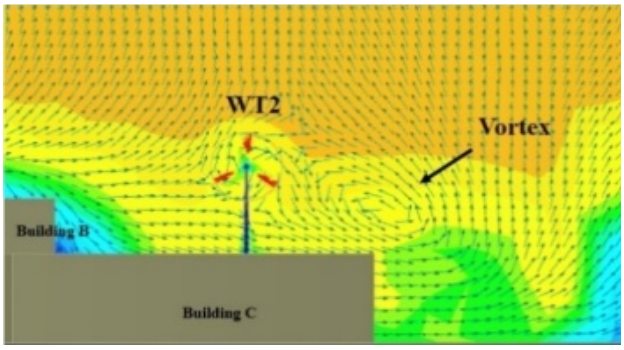

(b1) Vortex flow at WT2 as wind flows from NE

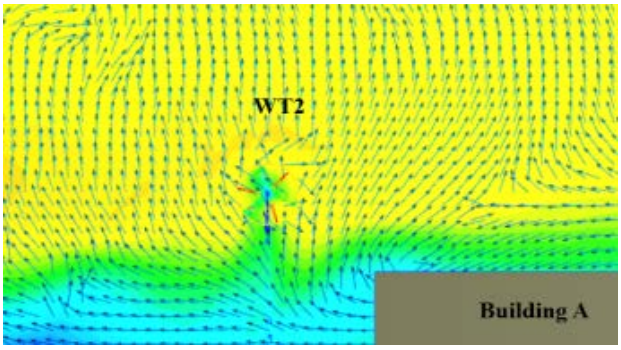

(b2) Vortex flow at WT2 as wind flows from SW

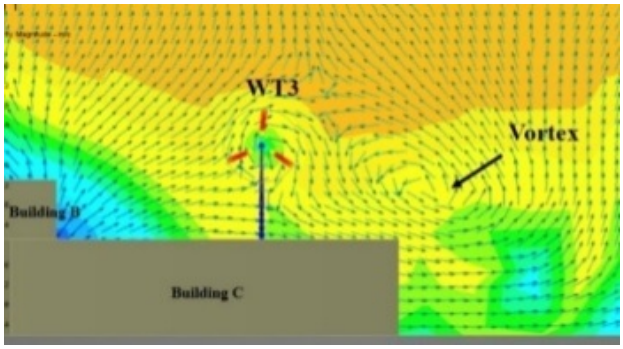

(c1) Vortex flow at WT3 as wind flows from NE

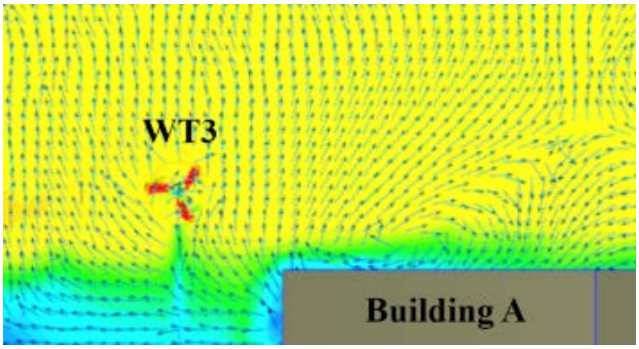

(c2) Vortex flow at WT3 as wind flows from SW

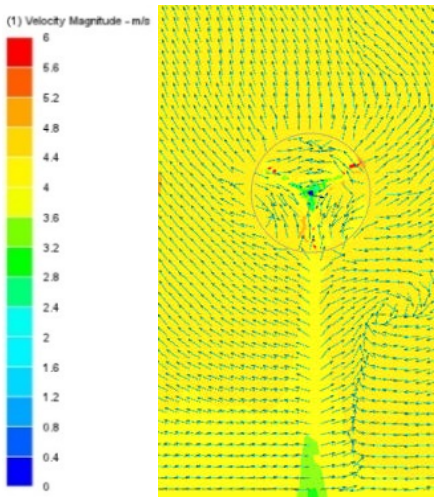

(d) No vortex flow at WT0, as the wind flows from both directions

Fig. 17. (a)–(d) Vortex-flow vectors to wind turbines from two directions.

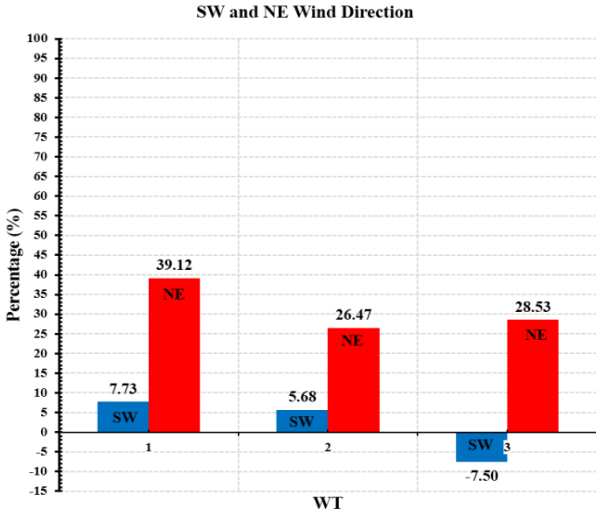

Fig. 18. Relative free spinning rotating of wind turbines WT1–WT3 compared to WT0, as the wind flows from NE and SW.

Table 6. Relative free spinning rotating of wind turbines WT1–WT3 compared to WT0, as the wind flows from NE and SW.

Wind Turbine No.	Effect of Wind Turbine Power (NE), (%)	Effect of Wind Turbine Power (SW), (%)
WT0	100.00	100.00
WT1	+39.12	+7.73
WT2	+26.47	+5.68
WT3	+28.53	-7.50

4.2 CFD Simulation Results

The free spinning rotating effect of the wind turbines as shown in Table 4 can be calculated as follows (using WT1 as the example as the wind flows from the SW):

$$\frac{x_i}{100} = \frac{N_{WT0} - N_{WT1}}{N_{WT0}}$$

$$\frac{x_i}{100} = \frac{216 - 200}{216}$$

$$x_i = +7.73\% \quad (15)$$

Figure 18 and Table 6 are the results of CFD k-Ɛ turbulence model simulation as the wind flow from both directions show the relative free spinning rotating of wind turbines WT1–WT3, as they increase and decrease in comparison to the unobstructed wind turbine, WT0, from both wind-flow directions. This occurs as the power performance of the wind turbine depends on the torque and the angular velocity of the rotor. As high angular velocity means high power and this study uses CFD method only for investigation in the free spin rotor condition, the angular velocity of the turbine is result of the power performance of the wind turbines.

The highest wind-turbine free spinning rotating is generated on WT1 as the wind flows from the NE, while the lowest wind-turbine free spinning rotating is generated on WT3 as the wind flows from the SW. As a result, the highest wind-turbine free spinning rotating

can be generated after the wind flows across the building to WT1 from the NE

The wind-turbine free spinning rotating of WT1, WT2, and WT3 compared to WT0 from the two directions are as follows.

When comparing WT1–WT3 with WT0 as the wind flows from the NE, the free spinning rotating of WT1, WT2, and WT3 is higher than the wind free spinning rotating of WT0 by 39.12%, 26.47%, and 28.53%, respectively.

When comparing WT1–WT3 with WT0 as the wind flows from the SW, the free spinning rotating of WT1 and WT2 is higher than the free spinning rotating of WT0 by 7.73% and 5.68%, respectively, while the free spinning rotating of WT3 is lower than the free spinning rotating of WT0 by 7.50%.

When comparing WT1–WT3 from different wind-flow directions, the performance of WT1–WT3 as the wind flows from the NE is higher than when the wind flows from the SW by 31.39%, 20.79%, and 36.03%, respectively.

4.3 CFD Results Discussions

Normally, the geometric features of the buildings and their layouts have major effects on wind turbines' power performance. The buildings create turbulence and cause unexpected changes in the wind's speed, direction, and frequency. In addition, the geometric features of the buildings can decrease the wind speed; however, they can also channel the wind flow into the buildings' canyon and lead to an increase in the wind speed because the Venturi effect can cause a wind-flow overpressure between buildings, which can increase the frequency of turbulent winds. If the temperature increases within the building-obstructed area, it can create a low-pressure cell and lead to increased wind speed and frequency. Moreover, widely spaced buildings can act as single isolated blocks; therefore, if the gap decreases between the buildings, the wind flow will likely become more prone to overpressure. Thus, the Venturi effect can change the airflow frequencies by producing a complex pattern of changes in the wind direction and speed.

When compared to WT0, the incoming wind flow from the NE creates a Venturi effect by channelling the incoming wind flow into the building canyons between buildings B-C and buildings C-D. Moreover, buildings A, B and C create a steep wind-shear gradient that leads to an increase in WT1–WT3 free spinning rotating by 39.12%, 26.47%, and 28.53%, respectively.

On the other hand, the incoming wind flow from the SW creates a Venturi effect by channelling the incoming wind flow into the building canyon between the buildings A-B. Further, building A creates a steep wind-shear gradient that leads to increased free spinning rotating of WT1 and WT2, by 7.73% and 5.68%, respectively, while the free spinning rotating of WT3 is decreased by 7.50%, since WT3 is not in the buildings canyon of the incoming wind flow. However, building A increases the vortex-flow effect to WT3.

4.4 Site Estimated Results

Figure 19 and Table 7 show the results of three 5-kW HAWTs' free spinning rotating derived from site measurement base on measured data as the wind flows from the SW at incoming wind speed of 4.5 m/s. The results show the free spinning rotating as WT1> WT3 > WT2, while the results from the CFD k-Ɛ turbulence model simulation show the free spinning rotating as WT1 > WT2 > WT3 as shown in Table 7.

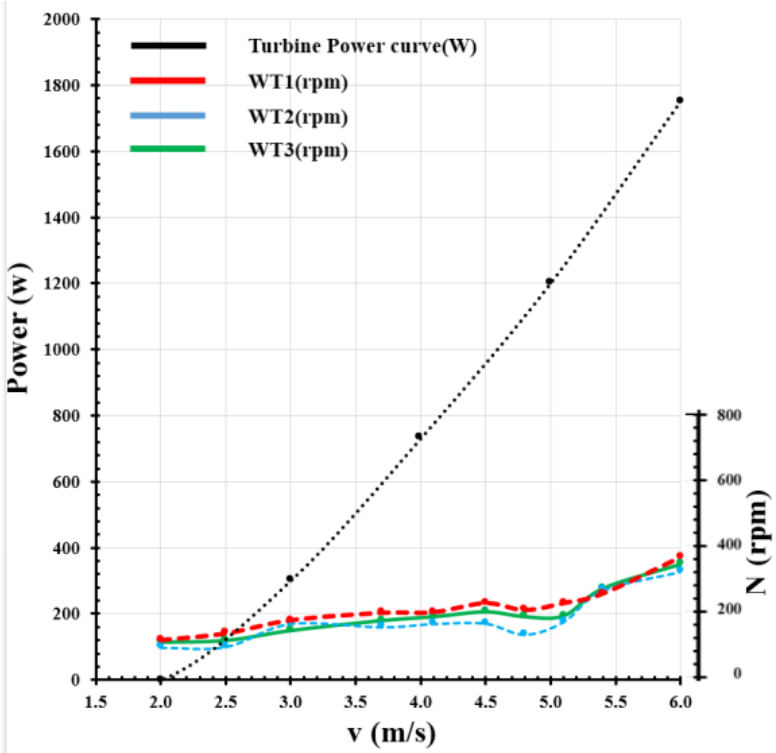

Fig. 19. Three 5-kW HAWTs' power performance, free spinning condition, derived from site measurement as the wind flows from the SW with a 5-kW HAWTs' power curve.

Table 7. Results of blade rotor free spinning condition of wind turbines at incoming wind speed as wind flow from SW between CFD simulation and site measurement

Method	V, m/s	Max Value	Med. Value	Min. Value
CFD	3.0	WT1	WT2	WT3
	4.5	WT1	WT2	WT3
	6.0	WT1	WT2	WT3
Exp.	3.0	WT1	WT2	WT3
	4.5	WT1	WT3	WT2
	6.0	WT1	WT3	WT2

Fig. 20. Direction of wind turbine with usually getting turbulence wind flow in DETC.

4.5 Site Estimated Discussions

Figure 19 describes the experimental results of the site measurement based on the measured data of the rotors' spinning speed compared to a 5-kW HAWT Power curve. Normally, the power curve of a wind turbine is calculated by multiplying torque with the angular velocity ($P = T\omega$), but WT1, WT2, WT3 power curves in this study are measured only by using angular velocity (ω) that match with the CFD simulation in this study which only calculate the angular velocity. The CFD model was simulated by only two directions of the wind flow, the NE and the SW, while the site measurement condition cannot fix the direction of wind flow, conversely, the wind flow always change due to turbulence. Hence, the result of the wind flow in the site measurement condition will affect the power performance difference from CFD condition.

Table 7 describes the results of the free rotor spinning condition of the wind turbine speed as the wind flows from the SW at incoming wind speed as shown between the CFD results and site measurement results. As the CFD results, the value of rotor spinning of WT1 > WT2 >WT3 while the measurement results show the value of rotor spinning of WT1 > WT3 > WT2 due to the direction of the inlet wind flow in CFD condition, the SW, is fixed cause the turbine were not changed in various direction from turbulence while wind turbine of the site measurement conditions be change along turbulence direction as shown in Figure 20.

However, the site measurement technique could validate that using the CFD technique in a building-obstructed wind-flow area causes both increased and decreased power performance effects of the wind turbines.

5. CONCLUSIONS

With reference to the results and discussions of the CFD simulation and the site estimated or the site measurement based on the measured data above, the conclusions are as follows:

1. The results of this CFD investigation of wind turbines and their positions in the site can be applied to determine the appropriate parameters required to obtain higher wind-turbine plant factors in the design stage.
2. The wind-turbine free spinning rotating in building-obstructed wind-flow areas do not always produce a low energy yield, since the buildings may cause a Venturi effect and steep wind-shear gradient, which can increase the wind turbines' free spinning rotating.
3. When choosing a building-obstructed wind-flow area in which to install wind turbines, the geometric features of the obstructing buildings' layout are major factors to be considered, as they will shape the wind-flow pattern to the wind turbines. This is a fair evaluation because obstructive buildings can cause a positive Venturi effect to channel in the canyon and a steep shear gradient to increase the wind turbines' free spinning rotating.

4. The moving condition or the rotating region for wind turbines and rotational wind turbines should be included in the CFD boundary conditions model because of their ability to enhance the

REN21 renewable energy policy network for the 21century.,Renewables

accuracy of the simulation results.

5. The results of this CFD turbulence-model simulation technique not only correspond to the related theory, but the numerical results can also reliably predict the profile-curve tendencies of the wind turbines' power performance in the site.
6. This CFD technique can also be applied to decision-making for plant positioning, locating wind turbines on the best points of the site and estimating the wind-turbine plant factors in promising areas. Moreover, this technique can significantly save money and time. It can be applied to make reliable and capable tools for wind turbines' power-performance prediction, optimisation of wind turbines' locating points, optimizing the obstructive buildings' influence, projects' cost-benefit analyses, etc.
7. The results of CFD includes validating with site measurement base on measured data want to enhance high reliable. However, if possible when using CFD simulation as the same in this study, the various direction of wind flow in the site should be concerned in CFD method for enhancing reliable of the results.

ACKNOWLEDGEMENTS

The authors would like to thank all who assisted in this study, including the team at the Energy Research and Service Center, Faculty of Engineering, RMUTT, who supported the work and helped obtain a high-quality and accurate analysis. The first author is very grateful to his supervisor, Asst. Professor Wirachai Roynarin, for his patience and support in overcoming the numerous obstacles in the process of conducting the study. Additionally, the authors would like to thank all the friends who gave support and motivation. The first author would also like to thank his family for their spiritual encouragement throughout the process of writing this paper.

REFERENCES

[1] Global Status Report, 2016. Accessed from the World Wide Web: http://www.ren21.net/wp-content/uploads/2016/10/REN21_GSR2016_FullReport_en_11.pdf.

[2] Tabrizi A.B., Whale J., Lyons T., and Urmee T., 2013. Performance and safety of rooftop wind turbines: Use of CFD to gain insight into inflow conditions. *Renewable Energy* 67: 242-251.

[3] Choi N.J., Nam S.H., Kim J.S., Lee S.M., and Kim K.C., 2011. CFD study on power output and flow characteristics of 110 kW class BAWT. *Proceedings of the 2011 International Conference on High Performance Computing and Simulation, HPCS 2011*: 859–864.

[4] Kaldellis J.K. and D. Zafirakis. 2011. The wind energy evolution: A short review of a long history. *Renewable Energy* 36(7): 1887–1901.

[5] Sengupta A., Biswas A., Gupta R. and N. Srinagar., 2016. Vertical axis wind turbines in the built environment- A review. *ISESCO J. Sci. Technol*, 12: 1–4.

[6] Stankovic S., Campbell N. and Harries A., 2009 Urban Wind Energy, Earthscan. Accessed from the World Wide Web: http://isfahan.ir/dorsapax/userfiles/file/re.energy/wind.pdf.

[7] Li Q., 2016. Study on power performance for straight-bladed vertical axis wind turbine by field and wind tunnel test. *Renewable Energy* 90: 291–300.

[8] Li Q., Murata J., Endo M., Maeda T., and Kamada Y., 2016. Experimental and numerical investigation of the effect of turbulent inflow on a Horizontal Axis Wind Turbine (Part I: Power performance). *Renewable Energy* 113: 713–722.

[9] Balduzzi F., Bianchini A., Carnevale E.A., Ferrari L and Magnani S., 2011. Feasibility analysis of a Darrieus VAWT installation in the rooftop of a building. In the *Proceedings of the International Conference on Applied Energy*, May 2011, Perugia, Italy, pp. 3345–3358.

[10] Tabrizi A.B., Whale J., Lyons T., and Urmee T., 2014. Performance and safety of rooftop wind turbines: Use of CFD to gain insight into inflow conditions. *Renewable Energy* 67: 242–251.

[11] Burton T., Sharpe D., Jenkins N., and Bossanyi E., 2001. Wind Energy Handbook. John Wiley & Sons.

[12] Ledo L., Kosasih P.B., and Cooper P., 2011. Roof mounting site analysis for micro-wind turbines. *Renewable Energy* 36(5): 1379–1391.

[13] Tabrizi A.B., Whale, Lyons J., Urmee T., and Peinke J., 2017. Modelling the structural loading of a small wind turbine at a highly turbulent site via modifications to the Kaimal turbulence spectra. *Renewable Energy* 105: 288–300.

[14] Jeong M.-S., Kim S.-W., Lee I., and Yoo S.-J., 2014. Wake impacts on aerodynamic and aeroelastic behaviors of a horizontal axis wind turbine blade for sheared and turbulent. *Journal of Fluids and Structures Flow Conditions* 50: 66–78.

[15] Sedaghatizadeh N., Arjomandi M., Kelso R., Cazzolato B., and Ghayesh M.H., 2017. Modelling of wind turbine wake using large eddy simulation, RENE 9215.

[16] Audierne E., Elizondo J., Bergami L., Ibarra H., and Probst O., 2010. Analysis of the furling behavior of small wind turbines. Applied Energy 87: 2278–2292.

[17] Larwood S., 2001. Wind turbine wake measurements in the operating region of a tail vane. In the 39th American Institute of Aeronautics and Astronautics Inc. (AIAA) Aerospace Sciences meeting, Reno, Nevada, USA.

[18] International Electrotechnical Commision (IEC). 2005 *Wind turbines: Part 12.1 – power performance measurements of electricity producing wind turbines.* IEC Report No. 61400-12-1. Geneva, Switzerland.

[19] Pagnini L.C., Burlando M., and Repetto M.P., 2015. Experimental power curve of small-size wind turbines in turbulent urban environment. Applied Energy 154: 112–121.

[20] Blocken B., 2015. CFD Simulation of Wind Environmental Conditions over Natural Complex Terrain. Work. Trends Challenges Wind Energy Harvest.: 30–31.

[21] Danao L.A., 2012. *The Influence of Unsteady Wind on the Performance and Aerodynamics of Vertical Axis Wind Turbines.* PhD Dissertation, The University of Sheffield, United Kingdom: 1–258.

[22] Menter F.R., Langtry R., and Völker S., 2006. Transition modelling for general purpose CFD codes. Flow, Turbulence and Combustion 77(1–4): 277–303.

[23] Bachant P. and M. Wosnik., 2015. Effects of Reynolds number on the performance and near-wake dynamics of a vertical-axis cross-flow turbine. Switzerland: MDPI (Multidiciplinary Digital Publishing Institute).

[24] R. Beckers. 2006. *Small Wind Turbine Site Selection.* Accessed from the https://www.solacity.com/small-wind-turbine-site-selection.

[25] Spirn A.W., 1986. *Air Quality at Street-Level: Strategies For Urban Design.* Prepared for: Boston Redevelopment Authority, USA.

[26] Tabrizi A.B., Whale J., Lyons T., and Urmee T., 2014. Performance and safety of rooftop wind turbines: Use of CFD to gain insight into inflow conditions. Renewable Energy 67 :242-251.